Supplementary Document

The static photoluminescence (PL) spectrum of the 2D-MoS_2@0D-CCD heterostructures shows two distinct light-emission pathways, providing insights into carrier excitation and transitions (Fig. 1(a)). The features were categorized based on PL spectra from bare MoS_2 sheets and CCDs. In Fig. 1(a), we identify two exciton emissions: exciton A (684 nm) and exciton B (632 nm), from spin-split band-edge transitions at the K point. Additionally, the negatively charged trion (A^-, 695 nm), formed by exciton A and an extra electron, is observed, highlighting the luminescent behavior of few-layer MoS_2. Emission pathways from the CCD regions include defect-bound exciton (494 nm), defect-bound trion (541 nm), and direct electron-hole recombination at CCD cores (576 nm). Analyzing spectral positions (Fig. 1(b)), we find consistent peak positions across all PL spectra, indicating stable sources of photoemission, whether in pristine or heterostructure configurations.

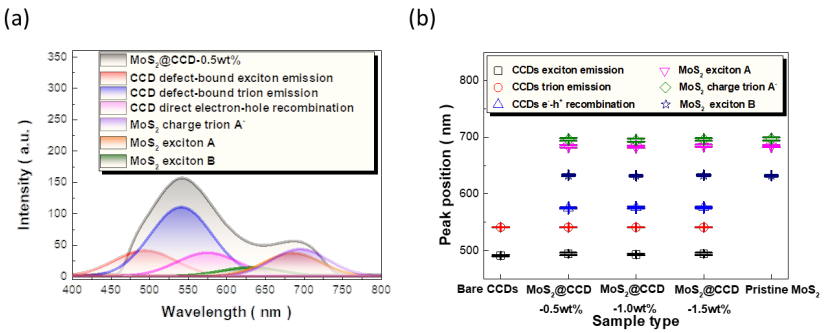

Fig.1 Spectral PL investigations of (a) MoS_2@CCD-0.5 wt% heterostructures reveal correlated features that have been deconvoluted and systematically indexed. Additionally, we conducted examinations on (b) the spectral positions.

Subsequently, to investigate and confirm the carrier transport behavior in the heterostructure, the photoluminescence (PL) enhancement factors (β) were evaluated.

$$\beta = (I_{HT,\ trion\ emission\ of\ CCD} - I_{bare\ CCD,\ trion\ emission\ of\ CCD})/(I_{bare\ CCD,\ trion\ emission\ of\ CCD}) x (A_{HT}/A_{CCD}) \quad (1)$$

Meanwhile, the intensity ratios of defect-bound trion to defect-bound exciton emissions and enhancement factors (β) results were presented in the Fig 2.(a)

We found that the reduction in PL enhancement of trion emission, indicated by a

suppressed β, is most significant in the MoS_2@CCD-1.0 wt% sample compared to MoS_2@CCD-0.5 wt%. This suggests that heterointerfaces enhance hole diffusion to the PEDOT:PSS matrix. The higher density of CCDs in MoS_2@CCD HTs (1.5 wt% CCDs) affects transfer channels, allowing holes to migrate to neighboring CCDs via hopping, which increases the β value due to additional radiative decay. In addition, we further confirmed the band structure diagram and designed the corresponding Si-based hybrid solar cell structures, as shown in Fig. 2(b) and Fig. 2(c). Subsequently, the performance of the devices was further confirmed through J-V measurements. Additionally, we introduced heat-stirred PEDOT:PSS into the device design as an improvement, which not only enhanced the electrical properties of the HTL but also effectively mitigated the effects of moisture. The results are shown in Fig. 2(d). These findings indicate that a specific composition ratio in the MoS_2@CCD HT design can optimize charge carrier transport and enhance carrier gain.

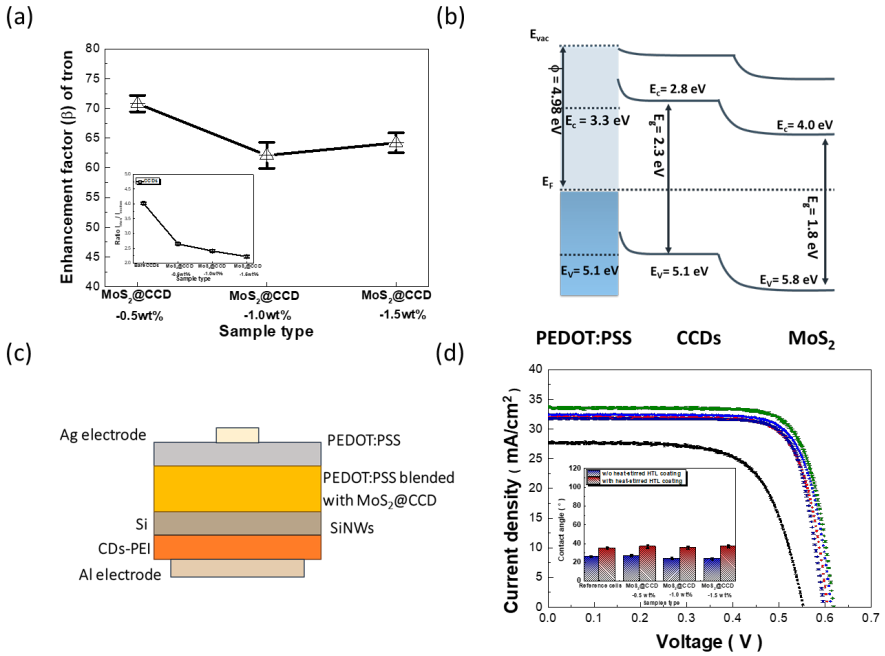

Fig. 2 (a) Evaluation of PL enhancement factors and the intensity ratio of defect-bound trion emission to defect-bound excitonic emission for each sample. (b) The band diagram of MoS2@CCD HTs blended with PEDOT:PSS films. (c) The schematic illustration of design hybrid solar cells. (d) Examinations of photovoltaic J–V characteristics. And the Surface wettability tests for the PEDOT:PSS HTLs with and without improvement via heat-stirred coatings, as the inset figure.